

Identifying the nature of dark matter at e^-e^+ colliders

Nabil Baouche^{1,2,*} and Amine Ahriche^{3,4,†}

¹*Laboratoire de Physique des Particules et Physique Statistique,*

Ecole Normale Supérieure, BP 92 Vieux Kouba, DZ-16050 Algiers, Algeria

²*Faculty of Technology, University of Dr. Yahia Fares-Medeia, DZ-26000 Medea, Algeria*

³*Department of Physics, University of Jijel, PB 98 Ouled Aissa, DZ-18000 Jijel, Algeria*

⁴*The Abdus Salam International Centre for Theoretical Physics, Strada Costiera 11, I-34014, Trieste, Italy*

In this work, we consider the process $e^+ + e^- \rightarrow b\bar{b} + \cancel{E}_T$, at the future electron-positron colliders such as the International Linear Collider and Compact Linear Collider, to look for the dark matter (DM) effect and identify its nature at two different centre-of-mass energies $E_{c.m.} = 500$ GeV and 1 TeV. For this purpose, we take two extensions of the standard model, in which the DM could be a real scalar or a heavy right-handed neutrino (RHN) similar to many models motivated by neutrino mass. In the latter extension, the charged leptons are coupled to the RHNs via a lepton flavor violating interaction that involves a charged singlet scalar. After discussing different constraints, we define a set of kinematical cuts that suppress the background, and generate different distributions that are useful in identifying the DM nature. The use of polarized beams (like the polarization $P(e^-, e^+) = [+0.8, -0.3]$ at the International Linear Collider) makes the signal detection easier and the DM identification more clear, where the statistical significance gets enhanced by twice (five times) for scalar (RHN) DM.

I. INTRODUCTION

The standard model (SM) has achieved a great success in describing the particle physics phenomenology at high energies, especially after the recent discovery at the LHC of a Higgs boson with mass around 125 GeV [1, 2], which is its most important success until now. Despite its successes, the SM is unable to explain many questions such as baryon asymmetry of the Universe, dark matter (DM), and neutrino masses and their mixing. Indeed, the first strong experimental evidence that the SM is complete was the neutrino oscillation observation [3].

One of the popular mechanisms to explain the smallness of neutrino masses is the so-called seesaw mechanism [4]. Another approach is based on getting naturally small neutrino masses radiatively, where the loop suppression factor, $1/(16\pi^2)^n$, makes the suppression natural instead of a suppression by a large scale of new physics (NP) [5–12] (for a review, see Ref [13]). Some of these models address, in addition to neutrino oscillation data, the DM problem in which a heavy right-handed neutrino (RHN) with a mass range from GeV to TeV can play the role of a good DM candidate [7, 10, 11, 14, 15]. These models predict an interesting signature at collider experiments [16–18]. For instance, in Ref. [18], the authors have probed the interactions of RHN with charged leptons via a singlet charged scalar by considering many final states at e^-e^+ colliders such as $\ell\ell + \cancel{E}_T$, $\ell\ell + \gamma + \cancel{E}_T$ and $\gamma + \cancel{E}_T$. This analysis was performed by taking into account all constraints: lepton flavor violating (LFV) processes, the muon anomalous magnetic moment [19], relic density, and the monophoton negative searches at LEP-II [20].

The International Linear Collider (ILC) and the Compact Linear Collider (CLIC) were proposed to discover physics beyond the SM, where the ILC can scan the c.m. energies from 250 to 500 GeV, with a possible expandability to 1 TeV [21–23], and the CLIC is subject to development with c.m. energies from 380 GeV to 3 TeV, with luminosity up to $2000 fb^{-1}$ [24]. The leptonic collider has the option of polarized beams, which may lead to an increasing signal/background ratio, and therefore enhances the NP signal strength. This could provide a valuable opportunity to detect new particles and determine their properties. In Ref. [25], it has been found that the b-tagging efficiency is about 80% when the misidentification efficiencies for the c jet and u/d/s jet are below 10% and 1%, respectively. This motivates any analysis that involves b jets. For instance, in Ref. [26], it has been shown that by considering the final state $b\bar{b} + \cancel{E}_T$ at the ILC, the hWW coupling can be measured at a precision of 4.8% and 1.2% at 250 and 500 GeV, respectively. This analysis was performed using the beams polarization $P(e^-, e^+) = [+0.8, -0.3]$.

Another approach to dealing with the DM problem is to extend the SM with singlet scalar(s), which plays a DM candidate role. This scalar is assigned by a global Z_2 symmetry in order to ensure the DM stability [27, 28].

*Electronic address: baouche.nabil@gmail.com

†Electronic address: aahriche@daad-alumni.de

Whatever the DM nature is, when a DM pair is produced, it does not leave any signature or trace at the detectors and behaves as missing energy. If one considers the final state $jj + \cancel{E}_T$ at e^-e^+ colliders such as the ILC or CLIC, where $\cancel{E}_T = DM + DM$, then the dijet may come from the Z/γ^* -gauge boson and/or the Higgs depending on the model considered: SM, scalar DM, or RHN DM. So, if the dijet is coming from the Higgs, then it would be suppressed except for the b jets. Therefore, we will consider here only b-tagged jets that can come from $Z/\gamma^*/Higgs$ according to the model and use the polarization to identify the DM nature. So, in this work, we will consider the signal $e^-e^+ \rightarrow b\bar{b} + \cancel{E}_T$ and try to propose relevant cuts that reduce the background and identify the DM nature based on the distributions shape with respect to the background.

This paper is organized as follows. In Sec-II, we describe the models and different current experimental constraints such as invisible Higgs decay, the muon anomalous magnetic moment, lepton flavor violation, DM relic density $\Omega_{DM}h^2$, and the LEP-II data. We propose different values for the model parameters, taking into account different bounds. In Sec-III, we describe the investigated process in detail, and we discuss our results in Sec-IV, where we consider the cases with polarized and unpolarized beams. Finally, we give our conclusion in Sec-V.

II. DM MODELS AND CONSTRAINTS

In this work, we will consider two types of models in which the DM could be either a real scalar or a heavy RHN. Therefore, we consider for the case of scalar DM a generic case of the Higgs portal [29], and in the case of heavy RHNs, we propose the SM extended with three heavy RHNs, $N_i (i = 1, 2, 3)$, and an electrically charged scalar field, S^\pm , which is a singlet under the $SU(2)_L$ gauge group. In addition, to ensure the DM candidate stability, we impose a global discrete \mathbb{Z}_2 symmetry, under which $\{S, N_i\} \rightarrow \{-S, -N_i\}$ and all other fields are even [17].

A. Scalar dark matter

We consider a very simple extension of the SM by adding a real singlet scalar defined under $SU(3)_C \otimes SU(2)_L \otimes U(1)_Y$ as $\phi \sim (1, 1, 0)$. This scalar field has to obey a global \mathbb{Z}_2 symmetry and should not develop a vacuum expectation value (vev), and therefore it could be a weakly interacting massive particle. In this setup, the DM candidate can self-annihilate into SM particles final states via the Higgs mediation. According to the scalar field mass and its coupling to Higgs, one can get the relic density and avoid the direct detection cross section bound.¹ The Lagrangian reads

$$\mathcal{L} = \mathcal{L}_{SM} + \frac{1}{2}\partial^\mu\phi\partial_\mu\phi - V(\phi, H), \quad (1)$$

where H is the SM Higgs doublet and $V(\phi, H)$ is the scalar potential, which after the electroweak symmetry breaking reads

$$V(\phi, h) \supset \frac{1}{2}m_\phi^2\phi^2 + \frac{c_s v}{2}h\phi^2, \quad (2)$$

with m_ϕ the real scalar mass after the symmetry breaking, c_s the quartic coupling constant of the potential term $\phi^2|H|^2$, $v = 246$ GeV the SM doublet vev, and h the usual SM Higgs field. So, the model is defined just by two free parameters: the coupling constant c_s and the scalar mass m_ϕ . At an electron-positron collider, it is possible to produce the real singlet scalar ϕ via the Z fusion $e^-e^+ \rightarrow e^-e^+h \rightarrow e^-e^+\phi\phi$, or by the associate production $e^-e^+ \rightarrow Zh \rightarrow Z\phi\phi$, where the Z gauge boson subsequently decays, primarily hadronically [30]. If the Higgs decay into invisible channel $h \rightarrow \phi\phi$, the decay width is given by

$$\Gamma_{inv}(h \rightarrow \phi\phi) = \frac{c_s^2 v^2}{32\pi m_h} \left(1 - \frac{4m_\phi^2}{m_h^2}\right)^{\frac{1}{2}}. \quad (3)$$

¹ By adding another scalar to the SM that assists the electroweak symmetry breaking, one can easily avoid the direct detection bound [28].

Model	Parameters
M_1	$\{m_\phi, c_s\} = \{10 \text{ GeV}, 1.25 \times 10^{-2}\}$,
M_2	$\{m_\phi, c_s\} = \{60 \text{ GeV}, 2.35 \times 10^{-2}\}$.

TABLE I: The parameters values for model 1 and model 2.

LFV process	Current bound
$\mathcal{B}(\mu \rightarrow e + \gamma)$	4.2×10^{-13} [37]
$\mathcal{B}(\tau \rightarrow \mu + \gamma)$	4.4×10^{-8} [30]
$\mathcal{B}(\tau \rightarrow e + \gamma)$	3.3×10^{-8} [38]
$\mathcal{B}(\tau \rightarrow e^- + e^+ + e^-)$	2.7×10^{-8} [39]
$\mathcal{B}(\mu \rightarrow e^- + e^+ + e^-)$	1.0×10^{-12} [40]
$\mathcal{B}(\tau \rightarrow \mu^- + \mu^+ + \mu^-)$	2.1×10^{-8} [39]

TABLE II: The current bounds for different LFV observables.

The experimental constraint on the invisible Higgs decay reads

$$\mathcal{B}_{inv}(h \rightarrow \phi\phi) = \frac{\Gamma_{inv}}{\Gamma_{inv} + \Gamma_{SM}^{tot}} \leq 0.16, \quad (4)$$

where $\Gamma_{SM}^{tot} = 4.20 \text{ MeV}$ is the SM Higgs total width [31]. This bound can be translated into a constraint on the couplings c_s and the scalar mass m_ϕ as

$$c_s \leq 1.2882 \times 10^{-2} \left(1 - \left(\frac{m_\phi}{62.5 \text{ GeV}} \right)^2 \right)^{-\frac{1}{4}}. \quad (5)$$

In our analysis, we focus on the case in which the scalars are pair produced through an on-shell Higgs decay. This means that we will consider the light masses range $m_\phi \leq m_h/2$, and we choose two values of the model free parameters $\{m_\phi, c_s\}$, where they respect the experimental constraint (4). We call them model 1 (M_1) and model 2 (M_2).

B. Fermionic dark matter

In this case, the SM was extended with an electrically charged singlet scalar field $S^+ \sim (1, 1, 2)$ and three RHNs, $N_i \sim (1, 1, 0)$ [10]. The Lagrangian has the form [32]

$$\mathcal{L} = \mathcal{L}_{SM} + \{g_{i\alpha} N_i^C \ell_{\alpha R} S^+ + \frac{1}{2} m_{N_i} N_i^C N_i + h.c\} - V, \quad (6)$$

where $\ell_{\alpha R}$ is the right-handed charged lepton, m_{N_i} are the heavy RHN's masses, C denotes the charge conjugation operator, and $g_{i\alpha}$ are the new Yukawa couplings. Here, V is the scalar potential. The Greek letters denote $\alpha = \mu, e, \tau$, and the fermion generations are labelled by $i = 1, 2, 3$. When the \mathbb{Z}_2 symmetry is imposed, the lightest RHNs becomes stable and could be a good DM candidate [10, 33]. These couplings as well the RHNs and the charged scalar masses enter the expression of the neutrino mass matrix elements depending on the model details.

The interactions (6) induce a new contribution to the muon's anomalous magnetic moment and LFV processes such as $\ell_\alpha \rightarrow \ell_\beta + \gamma$ and $\ell_\alpha \rightarrow \ell_\beta + \bar{\ell}_\beta + \ell_\beta$, and all are generated at one loop via the exchange of the charged scalar S^\pm , where the branching ratios are given in Refs [15, 34, 35]. Unlike other models [36], the contribution to the muon anomalous magnetic moments in this model is negative [15], and therefore does not to close the gap between the experimental measurement and the SM prediction $\delta a_\mu = a_\mu^{exp} - a_\mu^{SM} = 288(63)(43) \times 10^{-11}$ [30]. In Table II, we present the current bounds on different LFV observables.

The current experimental bounds in Table II must be fulfilled by the interactions (6), as well other bounds such as DM relic density if N_1 is considered as a DM candidate. If this is the case, the main annihilation channel

would be the S^\pm -mediated process $N_1 N_1 \rightarrow \ell_\alpha \ell_\beta$. In case in which there exist other annihilation channels,² an extra contribution to the total annihilation cross section will affect the relic density value. Therefore, to take into account this case, one has to adjust the charged scalar mass and the new Yukawa couplings in order to ensure $\Omega_{DM} h^2 = 0.1186 \pm 0.0020$ [41].

In this work, we will focus on the process $e^- e^+ \rightarrow b\bar{b} + \cancel{E}_T$ considering unpolarized beams for two c.m. energies: $E_{c.m.} = 500$ GeV and 1 TeV. Then, we expand our analysis and discussion by using the different beam polarizations at the electron-positron linear colliders that can be available at the ILC and CLIC, where in SM, the process mentioned above has three subprocesses, in which the missing energy is the light SM neutrinos $\cancel{E}_T^{(SM)} \equiv \nu_\alpha \bar{\nu}_\alpha$, where $\alpha = \mu, e, \tau$. In the case of RHN DM, the heavier RHNs, $N_{2,3}$, are pair produced at the collider, and decay into pairs of charged leptons $\ell_{\alpha R} \ell_{\beta R}$ ($\alpha, \beta = \mu, e, \tau$) and a pair of DM $N_1 N_1$ via S^\pm -mediated processes.

If $m_{N_{1,2,3}} < m_S$, in this case $N_{2,3}$ has a three-body decay, and therefore may decay outside of the detector. In the inverse case $m_{N_1} < m_S < m_{N_{2,3}}$, $N_{2,3}$ has a two-body decay with a larger decay width and a smaller distance, which should be inside the detector. Then, the missing energy in the process $e^- e^+ \rightarrow b\bar{b} + \cancel{E}_T$ could be defined in the three cases as:

1. $\cancel{E}_T = N_1 N_1$, if N_2 and N_3 decays inside the detector,
2. $\cancel{E}_T = N_1 N_1, N_1 N_2, N_2 N_2$, if only N_2 decays outside the detector,
3. $\cancel{E}_T = N_1 N_1, N_1 N_2, N_1 N_3, N_2 N_2, N_2 N_3, N_3 N_3$, if all $N_{2,3}$ decay outside the detector.

To check whether these three cases correspond to $m_{N_{1,2,3}} < m_S$, $m_{N_{1,2}} < m_S < m_{N_3}$, and $m_{N_1} < m_S < m_{N_{2,3}}$, respectively, one should estimate the distance travelled by the heavier RHNs $N_{2,3}$.

The distance D_i travelled by the heavier RHNs N_i can be defined by

$$\frac{D_i}{1 \text{ c.m.}} = 1.98 \times 10^{-4} \left(\frac{\Gamma_i}{10^{-7} \text{ MeV}} \right)^{-1} \left(\frac{E_i^2}{m_{N_i}^2} - 1 \right)^{1/2}, \quad (7)$$

where Γ_i , m_{N_i} , and E_i are the heavy RHN's decays widths, masses, and energies respectively, and $i = 2, 3$. Here, the total decay width of N_i , Γ_i , is estimated using LANEHP/CALCHEP [42, 43].

In Fig. 1, we show the travelled distance D_i as a function of $m_{N_{2,3}}$ for the three aforementioned cases for 500 benchmark points that fulfil the muon anomalous magnetic moment and the LFV bounds on $\ell_\alpha \rightarrow \ell_\beta + \gamma$ and $\ell_\alpha \rightarrow \ell_\beta + \ell_\beta + \ell_\beta$.

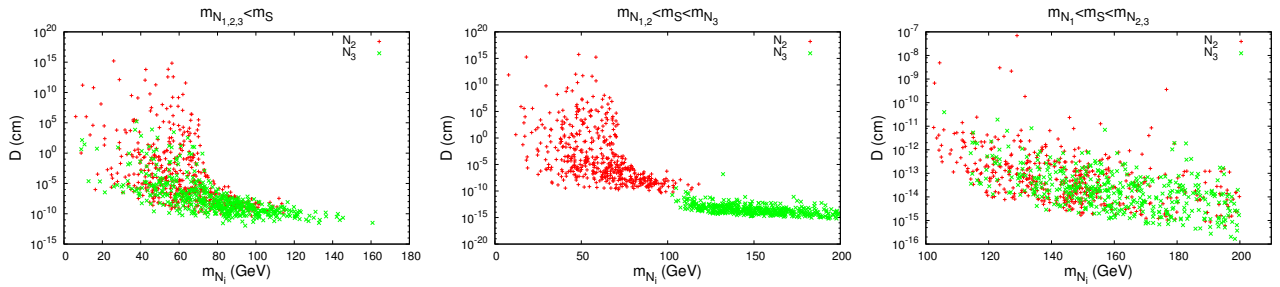


FIG. 1: The distance D_i travelled by the heavier RHNs as a function of their masses for the three cases: $m_{N_{1,2,3}} < m_S$ (left), $m_{N_{1,2}} < m_S < m_{N_3}$ (middle) and $m_{N_1} < m_S < m_{N_{2,3}}$ (right). Here, we consider the typical energy for $N_{2,3}$ to be 200 GeV.

It is clear from Fig. 1 that N_3 decays mostly inside the detector except for a few benchmark points in the case in which the charged scalar is the heaviest. For the RHN N_2 , it decays inside the detector in the case in which it is heavier than the charged scalar. In the inverse case, it could decay either inside or outside the detector depending on the couplings.

A search with a negative result had been performed by the L3 Collaboration at LEP-II about a single photon with a missing energy signal at c.m. energies 189 and 209 GeV with the corresponding luminosity values 176 and 130.2 pb^{-1} , respectively [20]. Based on this negative search, we will constrain our parameters space.

² Similar to the cases in Ref. [15].

Using LAMBERT [42] to implement the model (6) and CALCHEP [43] to compute the cross sections for the background $e^-e^+ \rightarrow \nu\bar{\nu}\gamma$ and the signal $e^-e^+ \rightarrow \gamma + \cancel{E}_T$, taking into account the same cuts used by LEP-II to search for the single photon events [20], we have the following:

- The polar angle of the photon is $|\cos\theta^\gamma| < 0.97$.
- The transverse momentum of photon must satisfy $p_T^\gamma > 0.02 E_{c.m.}$ (GeV).
- The energy of the photon must satisfy $E^\gamma > 1$ GeV.

At the end, we generate 3000 benchmark points that are in agreement with the bounds from the muon anomalous magnetic moment and the LFV processes $\ell_\alpha \rightarrow \ell_\beta + \gamma$ and $\ell_\alpha \rightarrow \ell_\beta + \bar{\ell}_\beta + \ell_\beta$. We distinguish two cases with $m_{N_i} = \{25, 30, 35 \text{ GeV}\}$ and $m_{N_i} = \{50, 60, 70 \text{ GeV}\}$. In Fig. 2, we display the significance of the signal $e^-e^+ \rightarrow \gamma + \cancel{E}_T$ (in the palette) for different values of the coupling $|g_{1e}|$ and the charged scalar mass for the two cases mentioned previously.

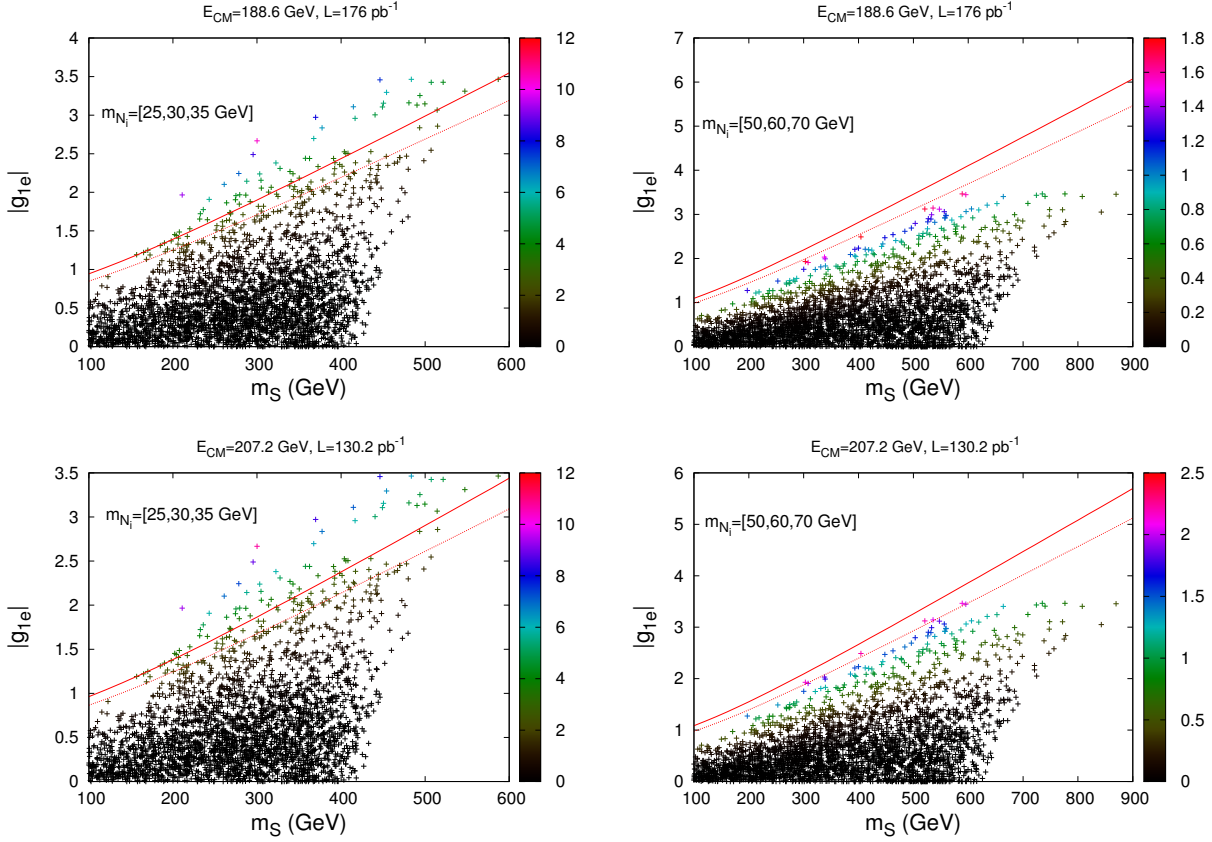


FIG. 2: The coupling $|g_{1e}|$ as a function of m_S for 3000 benchmark points with the two cases $m_{N_i} = \{25, 30, 35 \text{ GeV}\}$ (left) and $m_{N_i} = \{50, 60, 70 \text{ GeV}\}$ (right). The palette represents the signal significance S of the process $e^-e^+ \rightarrow \gamma + \cancel{E}_T$ for the c.m. energy values $E_{c.m.} = 188.6$ (up) and $E_{c.m.} = 207.2$ (down) with the integrated luminosity $L = 176 \text{ pb}^{-1}$ and $L = 130.2 \text{ pb}^{-1}$, respectively. The solid (dashed) line corresponds to the new constraint at LEP II, which makes the signal significance smaller than $S < 3$ ($S < 2$). For most of the benchmark points used here, the missing energy is identified as $\cancel{E}_T = N_1 N_1$, which justifies the choice of $|g_{1e}|$ in the y axes.

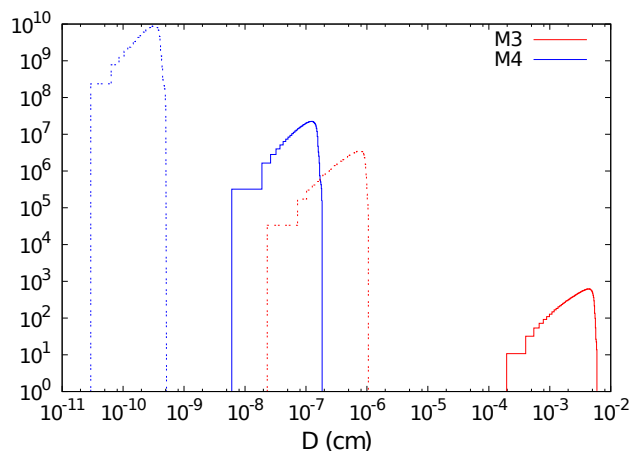
From Fig. 2, one can remark that once the LFV bounds are fulfilled the bound from LEP-II is also satisfied for N_1 heavier than 50 GeV, whereas LEP-II could exclude some benchmark points, especially using the analysis with $E_{c.m.} = 207.2$ GeV. For our analysis, we consider the following numerical values shown in Table III, which we call model 3 (M_3) and model 4 (M_4). These values respect the muon anomalous magnetic moment and LFV bounds in Table II.

In Fig. 3, the normalized distribution of the travelled distance D_i for the heavier RHNs $N_{2,3}$ is shown for $M_{3,4}$.

It is very clear that the travelled distance D_i is very small for both heavy RHNs $N_{2,3}$ since their decay via a three-body process $N_{2,3} \rightarrow N_1 + \ell_\alpha + \ell_\beta$ for both M_3 and M_4 . This means that they both decay inside the detector and can be accounted for missing energy, i.e., $\cancel{E}_T = N_1 N_1$.

Models		Parameters
M_3	m_{N_i} (GeV)	25.788, 28.885, 36.274,
	m_S (GeV)	196.75,
	$g_{i\alpha}/10^{-2}$	$\begin{pmatrix} 75.063 - i0.14367 & 0.0026819 - i0.015758 & -136.03i - 70.675 \\ -3.6203 - i35.9460 & -0.0035368 + i0.041316 & 120.47 - i286.100 \\ -3.0602 - i0.49553 & 0.057628 - i0.2462700 & -235.27 + i33.529 \end{pmatrix}$,
M_4	m_{N_i} (GeV)	62.184, 76.275, 95.736,
	m_S (GeV)	126.78,
	$g_{i\alpha}/10^{-2}$	$\begin{pmatrix} -60.008 + i2.4015 & -0.55187 - i1.1133 & -32.641 + i41.313 \\ 5.0213 + i22.533 & 3.5209 - i2.2480 & -112.35 - i32.473 \\ 4.2829 + i3.7764 & -2.2562 + i2.3886 & -171.25 - i94.890 \end{pmatrix}$.

TABLE III: The parameters values for model 3 and model 4.

FIG. 3: The normalized distribution of the travelled distance D_i (in cm) by the heavier RHNs N_2 (solid) and N_3 (dashed) at $E_{c.m.} = 500$ GeV.

III. FINAL STATE $b\bar{b} + \cancel{E}_T$ AT e^-e^+ COLLIDERS

The $m_h = 125.09$ GeV Higgs has the dominant decay mode $\mathcal{B}(h \rightarrow b\bar{b}) = 57.7\%$ [30], while the Z branching ratio $\mathcal{B}(Z \rightarrow b\bar{b}) = 15.12\%$ [30] is also significant. Then, the choice of the channel $b\bar{b} + \cancel{E}_T$ is interesting since the b-tagging efficiency is shown to be about 80% when the misidentification efficiencies for c jet and u/d/s jet are below 10% and 1%, respectively, at both the ILC and CLIC [25]. This is encouraging in considering the $b\bar{b}$ final state for our studied models M_i due to a possible clear signal. In this work, we want to probe the interactions (1) and (6) through the final state $b\bar{b} + \cancel{E}_T$ at a leptonic collider. This signal [Figs. 4(d) and 4(e)] has the background contributions $e^-e^+ \rightarrow Z(Z, h, \gamma^*) \rightarrow b\bar{b} + \cancel{E}_T$ [Fig. 4(a) and (b)] in addition to the W-fusion diagrams [Fig. 4(c)].

Future experiments such as the ILC [21, 22] and CILC [44, 45] may use polarized beams of electrons and positrons. This feature could help us to identify the DM nature whether it is fermionic, vectorial, or scalar. Here, we will consider both cases with and without polarized beams. By varying the c.m. energy in the range $250 \text{ GeV} < E_{c.m.} < 1 \text{ TeV}$, we get in Fig. 5 the cross section of different models and the background as a function of $E_{c.m.}$ with and without polarized beams.

One can see from Fig. 5 that the cross sections of M_1 and M_2 are identical for the cases with polarized and unpolarized beams. This feature is a numerical accident since the cross section is proportional to the Higgs invisible branching ratio $\mathcal{B}_{inv}(h \rightarrow \phi\phi)$, which has the same numerical value for M_1 and M_2 , so the aim of the choice in Table I is to find out the effect of the scalar mass m_ϕ and the coupling c_s . One notices also that the background cross section is increasing (decreasing) for the cases with the polarizations $P(e^-, e^+) = [0, 0]$ and $[-0.8, +0.3]$ ($P(e^-, e^+) = [+0.8, -0.3]$) as a function of the c.m. energy. This guides us to not consider the polarization $P(e^-, e^+) = [-0.8, +0.3]$ in our analysis. For M_3 and M_4 , the cross section is increasing with respect $E_{c.m.}$ especially within the polarization $P(e^-, e^+) = [+0.8, -0.3]$. Then, we will consider the c.m. energy values $E_{c.m.} = 500$ GeV and 1 TeV in the rest of our work.

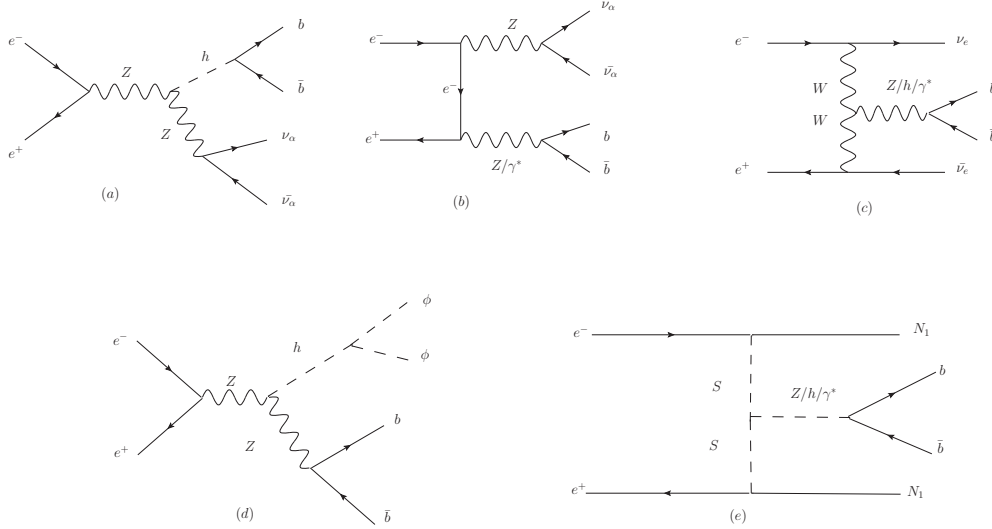


FIG. 4: The most important Feynman diagrams that contribute to background (a), (b), and (c) [(d) and (e)] [the signal] for the process $e^-e^+ \rightarrow b\bar{b} + \cancel{E}_T$.

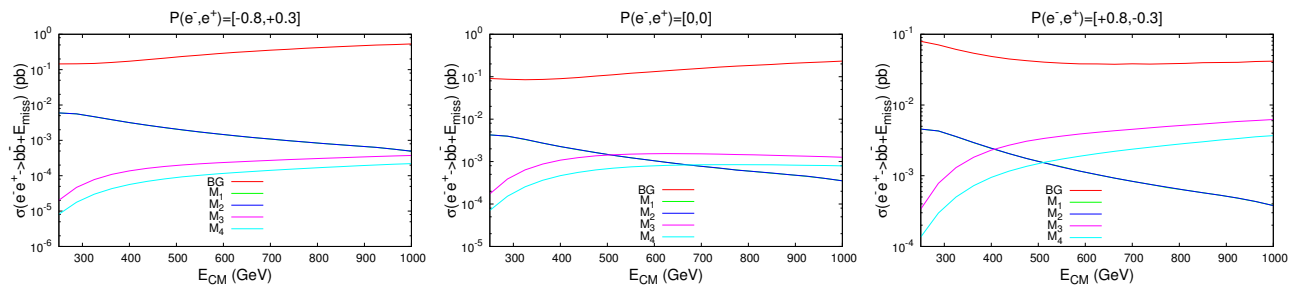


FIG. 5: The cross section of different models and background as a function of $E_{c.m.}$ with the polarization $P(e^-, e^+) = [-0.8, +0.3]$ (left) and $P(e^-, e^+) = [+0.8, -0.3]$ (right) and without polarization (middle). These figures are produced using the packages LANHEP/CALCHEP [42, 43].

The general signal significance definition is given by³ [46]

$$\mathcal{S} = \sqrt{2 \times [(N_S + N_{BG}) \times \log(1 + N_S/N_{BG}) - N_S]}, \quad (8)$$

where N_S and N_B are the signal and background events numbers, respectively. Here, N_S is given by

$$N_{S,BG} = \epsilon_b^2 \times \mathcal{L}_{int} \times \sigma_{S,BG}, \quad (9)$$

with $\epsilon_b = 0.8$ being the b-tagging efficiency factor, \mathcal{L}_{int} being the integrated luminosity, and $\sigma_{S,BG}$ being the signal or background cross section value.

IV. ANALYSIS AND DISCUSSION

In this work, we used LANHEP packages [42] to implement the models and generate their Feynman rules, and then we used CALCHep [43] to estimate the cross section and produce the differential cross section for the background and signal at both $E_{c.m.} = 500$ GeV and 1 TeV. To define the cuts on the kinematic variables that maximize the significance, we produced different distributions and looked for ranges in which the background

³ In Ref. [46], the authors used the notation \mathcal{Z}_0 for the significance, and here we use \mathcal{S} instead.

is reduced while keeping the signal value. Therefore, we generated different distributions, taking into account the following pre-cuts:

- The transverse momentum of the bottom quark (b) and the bottom antiquark (\bar{b}) must satisfy $p_T > 15$ GeV.
- The missing energy $\cancel{E}_T > 30$ GeV.
- The invariant mass of the bottom quark (b) and the bottom antiquark (\bar{b}) must be in the range $71 \text{ GeV} < M^{b,\bar{b}} < 145 \text{ GeV}$.
- The jet separation radius must satisfy $\Delta R_{b,\bar{b}} > 0.4$, where ΔR is given by

$$\Delta R = \sqrt{\Delta\phi^2 + \Delta\eta^2}, \quad (10)$$

where ϕ is the azimuthal angle and η is the pseudorapidity.

The first two cuts helped too much to reduce the contamination in the signal region. To ensure that the $b\bar{b}$ pair was produced through a Z -gauge boson and/or the Higgs as shown in Figs. 4(d) and 4 (e), we considered the third cut.

In the first step, we considered unpolarized beams of electrons and positrons to generate the differential cross section for the background (SM) and the signal (the models M_i) at both c.m. energies $E_{c.m.} = 500$ GeV and 1 TeV. Then, we looked for kinematical variables regions where the background was reduced and the signal was as maintained as possible. Then, the full set of cuts is given in Table IV.

$E_{c.m.}$	Selection cuts
500	$15 < p_T^b, 30 < \cancel{E}_T, 71 < M^{b,\bar{b}} < 145, 0.4 < \Delta R_{b,\bar{b}}, 90 \leq E_T^{b,\bar{b}} \leq 230, 210 \leq M_T^{b,\cancel{E}_T},$
1000	$15 < p_T^b, 30 < \cancel{E}_T, 71 < M^{b,\bar{b}} < 145, 0.4 < \Delta R_{b,\bar{b}}, 125 \leq E_T^{b,\bar{b}}, 240 \leq M_T^{b,\cancel{E}_T}.$

TABLE IV: The full set of cuts for the process $e^-e^+ \rightarrow b\bar{b} + \cancel{E}_T$ at both c.m. energies $E_{c.m.} = 500$ GeV and 1 TeV. Here, p_T^b is the transverse momentum of the bottom quark (b), \cancel{E}_T is the missing energy, $M^{b,\bar{b}}$ is the invariant mass of the bottom quark (b) and the bottom antiquark (\bar{b}), $\Delta R_{b,\bar{b}}$ is the jet cone angle, $E_T^{b,\bar{b}}$ is the transverse energy for the bottom quark (b) and bottom antiquark (\bar{b}), and M_T^{b,\cancel{E}_T} is the transverse mass of bottom-missing energy. All masses and energies are given in GeV.

A. Analysis using unpolarized beams

By imposing the full set of cuts in Table IV at both c.m. energies $E_{c.m.} = 500$ GeV, and 1 TeV, using unpolarized beams, we get the results shown in Table V.

$E_{c.m.}$ (GeV)	σ^{BG} (fb)	Models	σ^S (fb)	σ'^{BG} (fb)	σ'^S (fb)	\mathcal{S}_{100}	\mathcal{S}_{500}
500	108.19	M_1	1.475	17.804	0.520	0.9808	2.1936
		M_2	1.479		0.638	1.2024	2.6888
		M_3	1.425		0.956	1.7960	4.0168
		M_4	1.338		1.070	2.0088	4.4912
1000	233.27	M_1	0.352	49.072	0.282	0.3216	0.7192
		M_2	0.353		0.292	0.3328	0.7448
		M_3	1.265		0.942	1.0720	2.3976
		M_4	0.954		0.760	0.8656	1.9352

TABLE V: The cross section values of the background and the signal for each model within the pre-cuts σ^{BG} , σ^S and after applying the full cuts set given in Table IV σ'^S, σ'^{BG} at both c.m. energies $E_{c.m.} = 500$ GeV and 1 TeV. The corresponding signal significance is shown for the luminosity values $L = 100, 500 \text{ fb}^{-1}$.

Through the results presented in Table V, one notices that the signal cross section within the full set of cuts gets reduced a bit with respect to the case within the pre-cuts for all models at both $E_{c.m.} = 500$ GeV and 1 TeV, whereas, the background cross section gets reduced by about 83.5% (79%) at $E_{c.m.} = 500$ GeV ($E_{c.m.} = 1$ TeV). For luminosity $L = 100 \text{ fb}^{-1}$, we do not see any deviation from the SM at both $E_{c.m.} = 500$ GeV and 1 TeV. However, for $L = 500 \text{ fb}^{-1}$, one could notice a deviation from the SM at $E_{c.m.} = 500$ GeV for $M_{3,4}$. At $E_{c.m.} = 1$ TeV, within the same luminosity value, we could not even see a deviation from the SM for all models.

Therefore, for this c.m. energy, we require a large luminosity value (1 ab^{-1} or more) in order to see such a signal.

In case of large luminosity values that allow the signal to be seen, we show relevant normalized distributions in Figs. 6 and 7, for $E_{c.m.} = 500 \text{ GeV}$ and 1 TeV , respectively. The relevant distributions here are the polar angle between bottom-antibottom jets $\cos(\theta^{b,\bar{b}})$, the jet energy E^b , the jet transverse energy $E_T^b = \sqrt{m_b^2 + \vec{p}_T^2}$, the jet transverse momentum p_T^b , the transverse mass of the bottom-antibottom jets $M_T^{b,\bar{b}} = \sqrt{(E_T^b + E_T^{\bar{b}})^2 - (\vec{p}_T^b + \vec{p}_T^{\bar{b}})^2}$, the invariant mass of the missing energy with a jet M^{b,\cancel{E}_T} , the jet pseudorapidity η^b , the two-jet pseudo rapidity $\eta^{b,\bar{b}}$, and the polar angle between the two jets in the boost direction $\cos(\Theta^{b,\bar{b}})$.

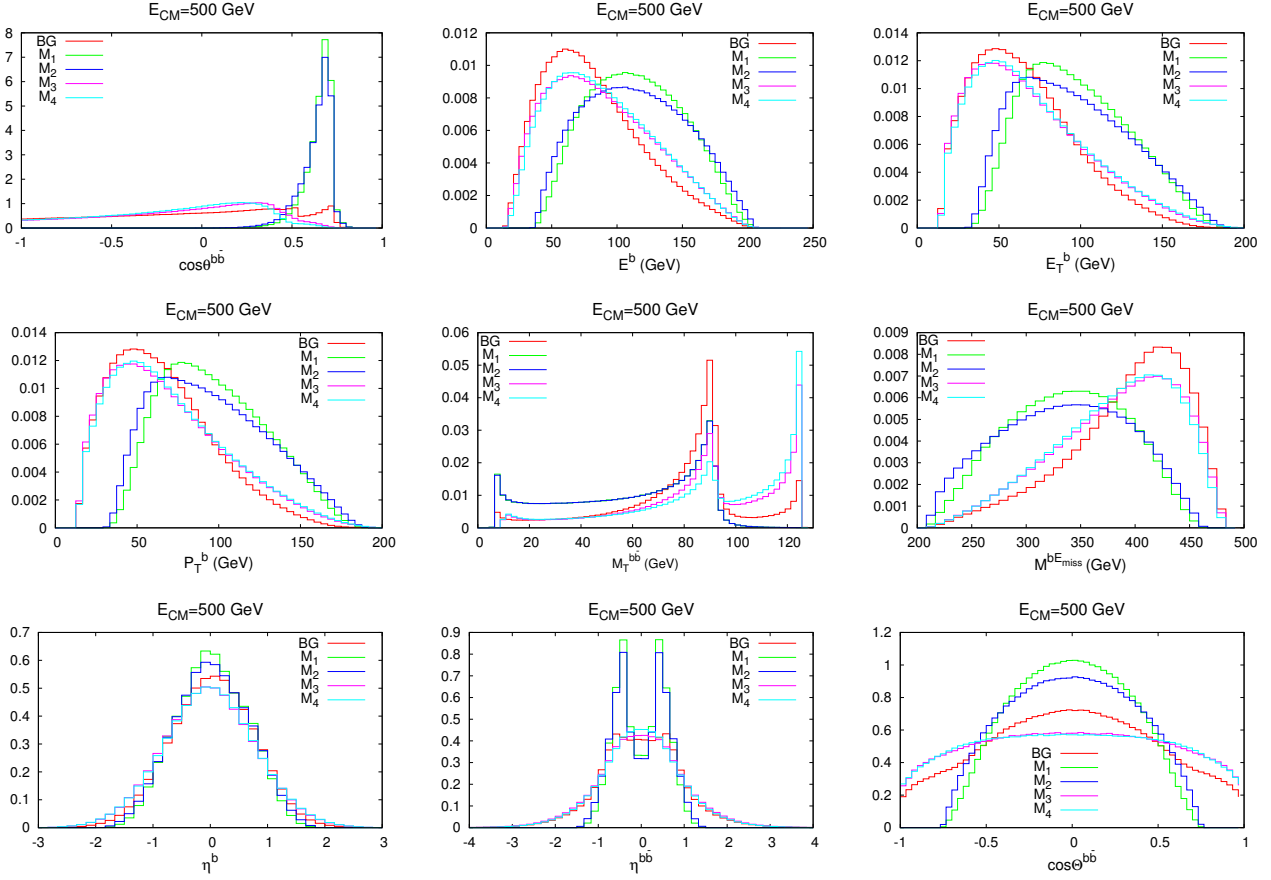


FIG. 6: The relevant normalized distributions of the process $e^- e^+ \rightarrow b\bar{b} + \cancel{E}_T$ at $E_{c.m.} = 500 \text{ GeV}$.

At $E_{c.m.} = 500 \text{ GeV}$ (Fig. 6), for scalar DM ($M_{1,2}$), the normalized distributions have different shapes with respect to both the background and the fermionic DM case ($M_{3,4}$), especially for the distributions $\cos(\theta^{b,\bar{b}})$, E^b , E_T^b , p_T^b , M^{b,\cancel{E}_T} , $\eta^{b,\bar{b}}$, and $\cos(\Theta^{b,\bar{b}})$. For the fermionic DM case ($M_{3,4}$), the normalized distributions have the same shape with respect to the background with a remarkable shift. For instance, if the DM is a scalar, the normalized distributions of $\cos(\theta^{b,\bar{b}})$ and $\eta^{b,\bar{b}}$ get maximized for $0.4 < \cos(\theta^{b,\bar{b}}) < 0.8$ and $0.3 < |\eta^{b,\bar{b}}| < 0.8$, respectively. However, at $E_{c.m.} = 1 \text{ TeV}$ (Fig. 7), the two cases of scalar and fermionic DM could be easily distinguished due to the different normalized distributions shapes.

B. Analysis using polarized beams

In search of new physics, the use of polarized beams at future electron/positron colliders such as the ILC and CLIC could reduce the background and/or enhance the signal [21–23]. The electron or positron polarization is defined as

$$P(f) = (N_{f_R} - N_{f_L}) / (N_{f_R} + N_{f_L}), \quad (11)$$

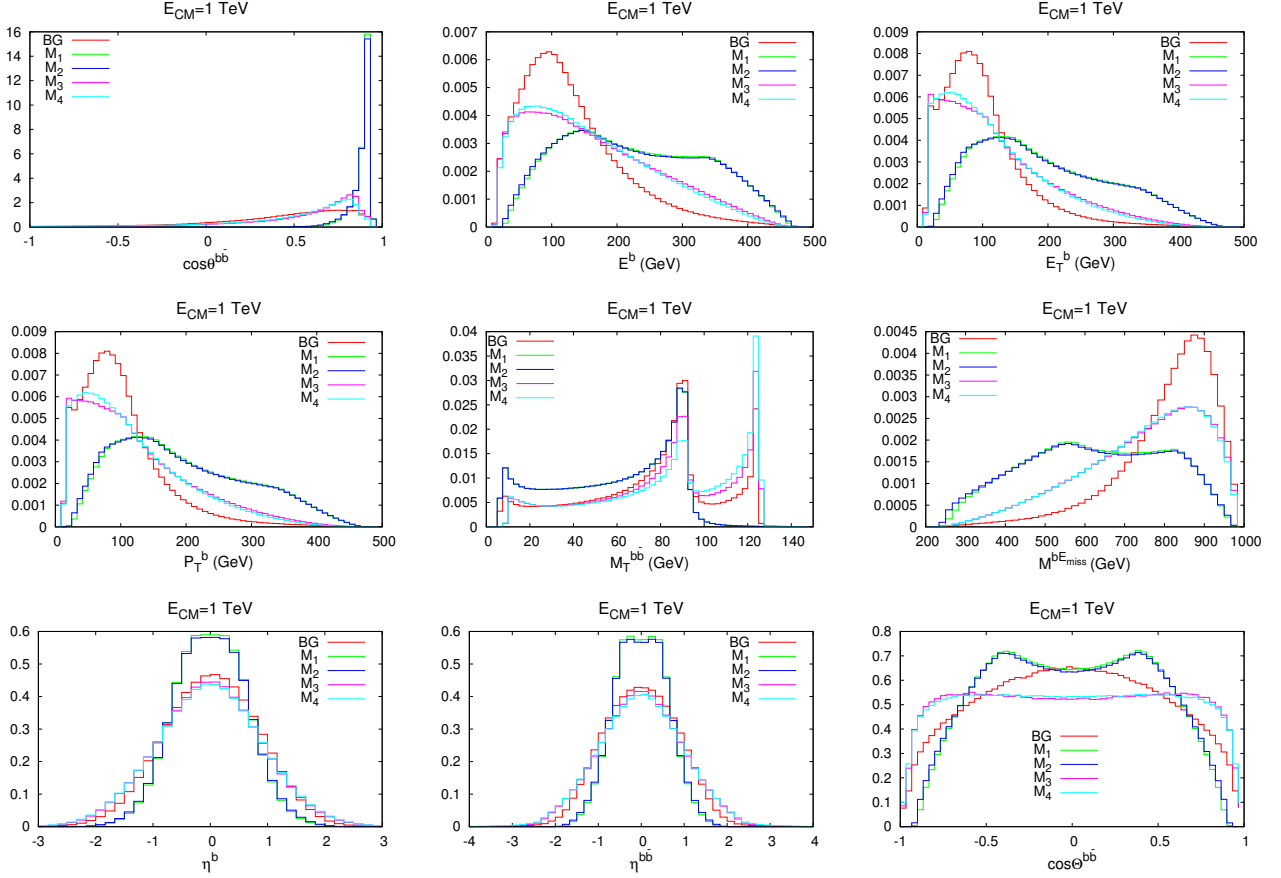


FIG. 7: The relevant normalized distributions of the process $e^-e^+ \rightarrow b\bar{b} + \cancel{E}_T$ at $E_{c.m.} = 1$ TeV.

where N_{f_R} (N_{f_L}) is the number of right- (left-) handed fermions. At the ILC, the polarization degree of the electron (positron) beams could reach 80% (30%), i.e., $|P(e^-)| < 0.80$ ($|P(e^+)| < 0.30$) [22]. The positron polarization could be improved up to 60% at the CLIC [44, 45].

Here, we reanalyze the same process at the same c.m. energy values within the polarization $P(e^-, e^+) = [+0.8, -0.3]$, while keeping the same full set of cuts given in Table IV. We present the results compared to the case without polarization in Table VI.

$E_{c.m.}$ (GeV)	$P(e^-, e^+) = [0, 0]$					$P(e^-, e^+) = [+0.8, -0.3]$			
	σ^{BG} (fb)	Models	σ^S (fb)	\mathcal{S}_{100}	\mathcal{S}_{500}	σ^{BG} (fb)	σ^S (fb)	\mathcal{S}_{100}	\mathcal{S}_{500}
500	17.804	M_1	0.520	0.9808	2.1936	5.061	0.558	1.9488	4.3584
		M_2	0.638	1.2024	2.6888		0.685	2.3832	5.3304
		M_3	0.956	1.7960	4.0168		2.166	7.2328	16.1736
		M_4	1.070	2.0088	4.4912		2.570	8.4944	18.9944
1000	49.072	M_1	0.282	0.3216	0.7192	9.950	0.303	0.7640	1.7096
		M_2	0.292	0.3328	0.7448		0.313	0.7896	1.7656
		M_3	0.942	1.0720	2.3976		5.472	12.8312	28.6912
		M_4	0.760	0.8656	1.9352		4.219	10.0520	22.4784

TABLE VI: The cross section values for the background σ^{BG} and the signal σ^S estimated for the considered energies within the full set of cuts given in Table IV, without and with polarized beams at both c.m. energies $E_{c.m.} = 500$ GeV and 1 TeV. The significances \mathcal{S}_{100} and \mathcal{S}_{500} correspond to the two integrated luminosity values $L = 100 fb^{-1}$ and $500 fb^{-1}$, respectively.

From Table VI, by comparing the cases with and without polarization, one remarks that the cross section value for the background σ^{BG} is reduced by about 72% (80%) at $E_{c.m.} = 500$ GeV ($E_{c.m.} = 1$ TeV). On the

contrary, the signal cross section value σ^S gets increased by about 7% for both $M_{1,2}$ at both c.m. energies $E_{c.m.} = 500$ GeV and 1 TeV. One can also see the cross section value for M_3 (M_4) gets raised by about 127% (140%) and by 481% (455%) for c.m. energies 500 GeV and 1 TeV respectively. Consequently, the signal significance gets enhanced by 303% (323%) and by 1097% (1061%) for M_3 (M_4) at 500 GeV and 1 TeV, respectively. When considering the polarization $P(e^-, e^+) = [+0.8, -0.3]$, the background cross section gets decreased sharply due to the vertices suppression of the electron-positron with gauge bosons unlike the vertices of the charged scalar-Majorana fermion-charged lepton (for $M_{3,4}$), which enhances the cross section.

For luminosity $L = 100 fb^{-1}$, one discovers for $M_{3,4}$ at both $E_{c.m.} = 500$ GeV and 1 TeV; however, for $L = 500 fb^{-1}$, one can see also a discovery for all models at $E_{c.m.} = 500$ GeV except Model 1. At $E_{c.m.} = 1$ TeV within the same luminosity, we could not even see a deviation from the SM for $M_{1,2}$, unlike $M_{3,4}$ in which one can clearly see a discovery. Therefore, we require a large luminosity value ($1 ab^{-1}$ or more) in order to see such a signal for two models $M_{1,2}$ in which DM is a scalar.

In Figs. 8 and 9, we show the relevant normalized distributions at $E_{c.m.} = 500$ GeV and 1 TeV, respectively, using the polarized beams $P(e^-, e^+) = [+0.8, -0.3]$.

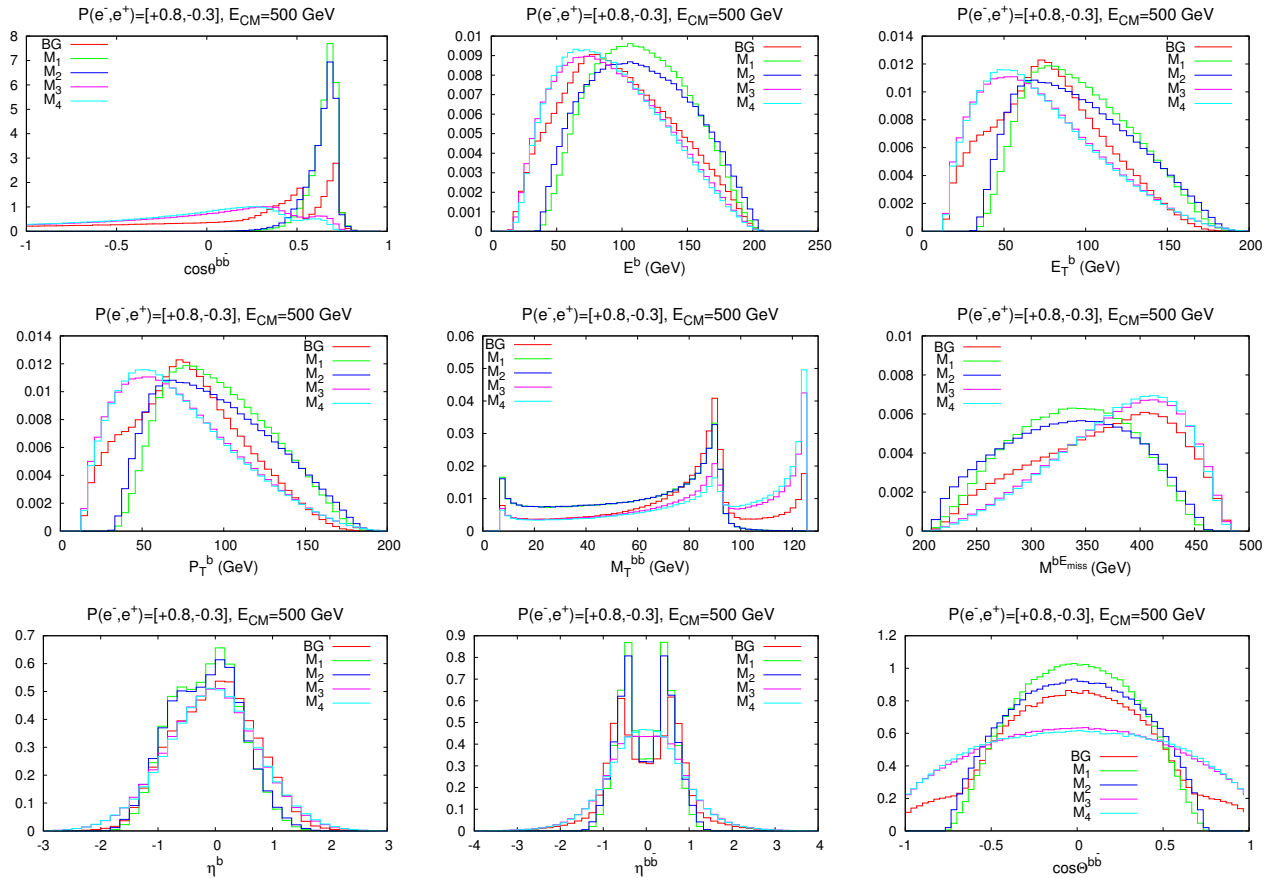


FIG. 8: The relevant normalized distributions of the process $e^- e^+ \rightarrow b\bar{b} + \cancel{E}_T$ at $E_{c.m.} = 500$ GeV with polarized beams $P(e^-, e^+) = [+0.8, -0.3]$.

From Fig. 8, for scalar DM ($M_{1,2}$), the normalized distributions have different shapes with respect to the background, especially for the distributions: E_T^b , p_T^b , M^{b, \cancel{E}_T} , η^b , and $\cos(\Theta^{b, \bar{b}})$. However, for fermionic DM ($M_{3,4}$), the distributions shape is different for $\cos(\theta^{b, \bar{b}})$, E^b , E_T^b , p_T^b , M^{b, \cancel{E}_T} , $\eta^{b, \bar{b}}$, and $\cos(\Theta^{b, \bar{b}})$. From Fig. 9, one notices that the normalized distributions E^b , E_T^b , p_T^b , M^{b, \cancel{E}_T} , and $\cos(\Theta^{b, \bar{b}})$ have different shapes between the background, the scalar DM ($M_{1,2}$), and the fermionic DM cases ($M_{3,4}$). One remarks also that for the background and the fermionic DM case ($M_{3,4}$) the normalized distributions have the same shape especially for $\cos(\theta^{b, \bar{b}})$, η^b , and $\eta^{b, \bar{b}}$.

By comparing the results produced at $E_{c.m.} = 500$ GeV using polarized beams (Fig. 8) with those without polarization (Fig. 6), one can notice a clear difference. For instance, if the DM is a scalar, the maximum of the normalized distributions of E^b , p_T^b , and η^b get shifted into $30 \text{ GeV} < E^b < 70 \text{ GeV}$, $15 \text{ GeV} < p_T^b < 65 \text{ GeV}$,

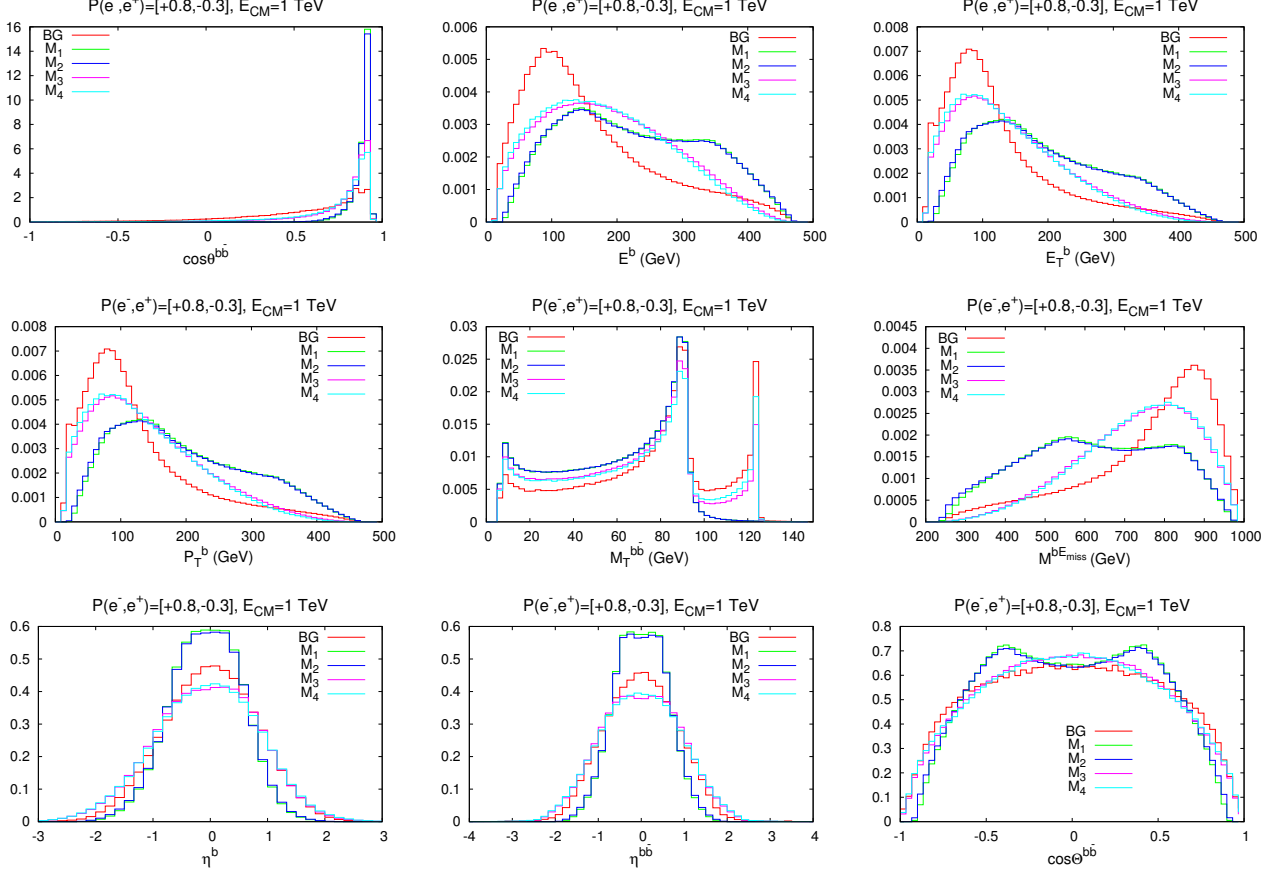


FIG. 9: The relevant normalized distributions of the process $e^-e^+ \rightarrow b\bar{b} + \cancel{E}_T$ at $E_{c.m.} = 1$ TeV with polarized beams $P(e^-, e^+) = [+0.8, -0.3]$.

and $-1 < \eta^b < 0.2$, respectively, with respect to the case without polarization. At $E_{c.m.} = 1$ TeV, for the fermionic DM case ($M_{3,4}$), the maximum of the normalized distributions of M^{b, \cancel{E}_T} and $|\cos(\Theta^{b, \bar{b}})|$ get shifted also into $450 \text{ GeV} < M^{b, \cancel{E}_T} < 780 \text{ GeV}$ and $|\cos(\Theta^{b, \bar{b}})| < 0.4$, respectively.

To get idea about the required values for the luminosity to observe such a deviation or a discovery, we estimate the signal significance by varying integrated luminosity values L . We show in Fig. 10 the signal significance for different models, using polarized and unpolarized beams

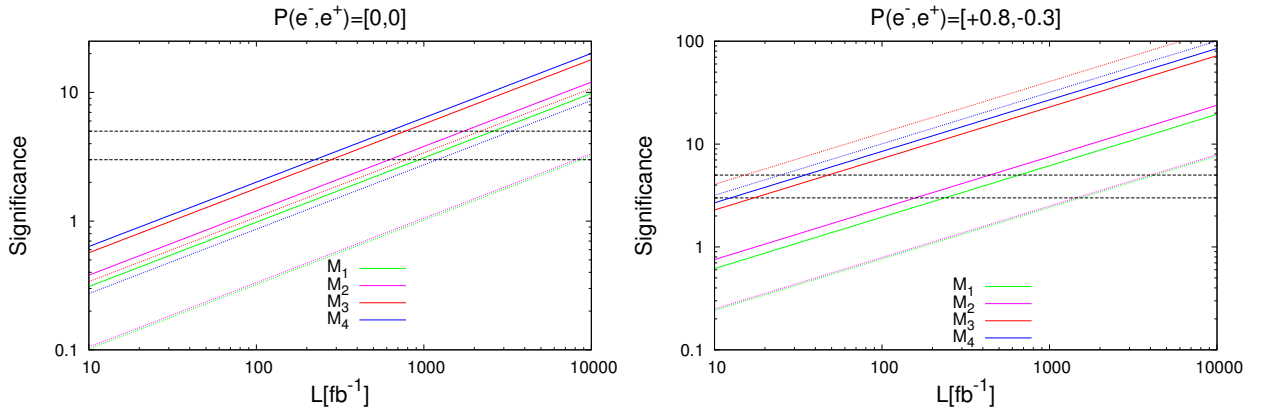


FIG. 10: The significance \mathcal{S} vs luminosity L at different c.m. energies (solid lines at 500 GeV, the dashed lines at 1 TeV) within the full set of cuts given in Table IV, without (left) and with (right) polarized beam. The two horizontal dashed lines represent $\mathcal{S} = 3$ and $\mathcal{S} = 5$, respectively.

From Fig. 10, one remarks easily that the use of polarized beams (with the polarization $P(e^-, e^+) = [+0.8, -0.3]$) makes the signal detected with smaller integrated luminosity as compared to the case with unpolarized beams for each model and at $E_{c.m.} = 500$ GeV, 1 TeV. For example, at $E_{c.m.} = 500$ GeV, a 5σ significance requires a minimal luminosity value 750 fb^{-1} (600 fb^{-1}) for M_3 (M_4) using unpolarized beams. Using polarized beams, this minimal luminosity value becomes 45 fb^{-1} (30 fb^{-1}) for M_3 (M_4). Similar remarks hold for the models $M_{1,2}$, where the required luminosity gets decreased from 2500 (1700) to 650 fb^{-1} (430 fb^{-1}) for M_1 (M_2).

In Table VII, we summarize the events number for the background and the signal for the different models using polarized and unpolarized beams at $E_{c.m.} = 500$ GeV and 1 TeV.

$E_{c.m.}$ (GeV)	$P(e^-, e^+) = [0, 0]$					$P(e^-, e^+) = [+0.8, -0.3]$			
	N_{BG}	Models	N_S	\mathcal{S}_{100}	\mathcal{S}_{500}	N_{BG}	N_S	\mathcal{S}_{100}	\mathcal{S}_{500}
500	1139.456	M_1	33.2864	0.9808	2.1936	323.904	35.7120	1.9488	4.3584
		M_2	40.8320	1.2024	2.6888		43.8400	2.3832	5.3304
		M_3	61.1840	1.7960	4.0168		138.6368	7.2328	16.1736
		M_4	68.4800	2.0088	4.4912		164.4864	8.4944	18.9944
1000	3140.608	M_1	18.0608	0.3216	0.7192	636.8064	19.4048	0.7648	1.7104
		M_2	18.6944	0.3328	0.7448		20.0320	0.7896	1.7656
		M_3	60.2880	1.0720	2.3976		350.2080	12.8312	28.6912
		M_4	48.6528	0.8656	1.9360		270.0224	10.0528	22.4784

TABLE VII: The background and signal events number N_{BG} , N_S estimated for the considered energies within the full set of cuts given in Table IV, without and with polarized beams at both c.m. energies $E_{c.m.} = 500$ GeV and 1 TeV. The significance \mathcal{S}_{100} and \mathcal{S}_{500} correspond to the two integrated luminosity values $L = 100$ and 500 fb^{-1} , respectively.

The results presented in Table VII give evidence that with the polarization $P(e^-, e^+) = [+0.8, -0.3]$ suppresses the background N_{BG} events number by 72% and by 80% for $E_{c.m.} = 500$ GeV and 1 TeV, respectively. Simultaneously, the signal N_S number of events for M_3 (M_4) gets improved by 127% (140%) and by 481% (455%) for c.m. energies 500 GeV and 1 TeV, respectively. This (significant) excess of events numbers could be an indication of the nature of DM; i.e., if the DM is a heavy RHN, the excess could be about five times.

V. CONCLUSIONS

In this work, we have investigated the possibility of detecting the signal significance of DM and identifying its nature. In our setup, the DM could be either a real scalar or heavy RHN produced at future electron-positron linear colliders such as the ILC and CLIC. To realize this task, we considered the process $e^-e^+ \rightarrow b\bar{b} + \cancel{E}_T$ at two different c.m. energies: $E_{c.m.} = 500$ GeV and 1 TeV. Here, we considered two parameter values sets for both scalar and RHN cases, four models, and we defined and investigated different experimental constraints for each case, such as the Higgs invisible decay, the muon anomalous magnetic moment, lepton flavor violation, DM relic density, and possible constraints from LEP-II. The latter constraint comes from the negative search of the monophoton at LEP-II, i.e., from the process $e^-e^+ \rightarrow \gamma + \cancel{E}_T$, which is translated into bounds on the DM and charged scalar masses and the Yukawa coupling $|g_{1e}|$.

We found that when using appropriate cuts (in Table IV), the background gets significantly decreased and the signal significance gets lifted especially for the heavy RHN DM case. Using unpolarized beams at $E_{c.m.} = 500$ GeV, the DM nature can be distinguished using the normalized distributions: E_T^b , p_T^b , M^{b,\cancel{E}_T} , $\eta^{b,\bar{b}}$, and $\cos(\Theta^{b,\bar{b}})$. However, a remarkable shift can be observed in most of the distributions for the fermionic DM case. At $E_{c.m.} = 1 \text{ TeV}$, the DM nature can be also distinguished whether it is scalar or fermionic using the different distributions.

Using polarized beams, the shape difference with respect to the background for most of the distributions is more clear, and smaller values of luminosity with respect of the case without polarized beams are required. Although, using the polarization $P(e^-, e^+) = [+0.8, -0.3]$, the background cross section gets suppressed by about 80%, and/or the signal one gets enhanced. This leads to a significant enhancement on the statistical significance by double if the DM is a scalar and by five times if the DM is a heavy RHN.

Acknowledgements

This work is supported by the Algerian Ministry of Higher Education and Scientific Research under the CNEPRU Project No. *B00L02UN180120140040*. N. Baouche thanks the ICTP where part of this project was realized for the warm hospitality. We want to thank Junping Tian for his useful comments and clarifications. We would like to thank Salah Nasri, Luigi Delle Rose, and Rikard Enberg for reading the manuscript and for their useful comments.

-
- [1] G. Aad *et al.* [ATLAS Collaboration], Phys. Lett. B **716**, 1 (2012) [arXiv:1207.7214 [hep-ex]]. I
- [2] S. Chatrchyan *et al.* [c.m.S Collaboration], Phys. Lett. B **716**, 30 (2012) [arXiv:1207.7235 [hep-ex]]. I
- [3] S. Fukuda *et al.* [Super-Kamiokande Collaboration], Phys. Rev. Lett. **86**, 5651 (2001) [hep-ex/0103032]. Q. R. Ahmad *et al.* [SNO Collaboration], Phys. Rev. Lett. **87**, 071301 (2001) [nucl-ex/0106015]. I
- [4] M. Gell-Mann, P. Ramond, and R. Slansky, in Supergravity, edited by P. van Nieuwenhuizen and D. Z. Freedman (North-Holland, Amsterdam, 1979), p. 315; T. Yanagida, in Proceedings of the Workshop on the Unified Theory and the Baryon Number in the Universe, edited by O. Sawada and A. Sugamoto, KEK Report No. 79-18 (Tsukuba, Japan, 1979), p. 95; R. N. Mohapatra and G. Senjanovic, Phys. Rev. Lett. **44**, 912 (1980). J. Schechter and J. W. F. Valle, Phys. Rev. D **22**, 2227 (1980). J. Schechter and J. W. F. Valle, Phys. Rev. D **25**, 774 (1982). I
- [5] T. P. Cheng and L. F. Li, Phys. Rev. D **22**, 2860 (1980). I
- [6] A. Zee, Phys. Lett. **93B**, 389 (1980) Erratum: [Phys. Lett. **95B**, 461 (1980)].
- [7] E. Ma, Phys. Rev. Lett. **81**, 1171 (1998) [hep-ph/9805219]. I
- [8] A. Zee, Nucl. Phys. B **264**, 99 (1986).
- [9] K. S. Babu, Phys. Lett. B **203**, 132 (1988).
- [10] L. M. Krauss, S. Nasri and M. Trodden, Phys. Rev. D **67**, 085002 (2003) [hep-ph/0210389]. I, II B, II B
- [11] M. Aoki, S. Kanemura and O. Seto, Phys. Rev. Lett. **102**, 051805 (2009) [arXiv:0807.0361 [hep-ph]]; M. Aoki, S. Kanemura and O. Seto, Phys. Rev. D **80**, 033007 (2009) [arXiv:0904.3829 [hep-ph]]. I
- [12] M. Gustafsson, J. M. No and M. A. Rivera, Phys. Rev. Lett. **110**, no. 21, 211802 (2013) Erratum: [Phys. Rev. Lett. **112**, no. 25, 259902 (2014)] [arXiv:1212.4806 [hep-ph]]. I
- [13] S. M. Boucenna, S. Morisi and J. W. F. Valle, Adv. High Energy Phys. **2014**, 831598 (2014) [arXiv:1404.3751 [hep-ph]]; Y. Cai, J. Herrero-Garcia, M. A. Schmidt, A. Vicente and R. R. Volkas, arXiv:1706.08524 [hep-ph]. I
- [14] H. Okada and K. Yagyu, Phys. Rev. D **93**, no. 1, 013004 (2016) [arXiv:1508.01046 [hep-ph]]; L. G. Jin, R. Tang and F. Zhang, Phys. Lett. B **741**, 163 (2015) [arXiv:1501.02020 [hep-ph]]; K. Cheung, T. Nomura and H. Okada, arXiv:1610.04986 [hep-ph]; S. Baek, H. Okada and T. Toma, JCAP **1406**, 027 (2014) [arXiv:1312.3761 [hep-ph]]; S. Kashiwase, H. Okada, Y. Orikasa and T. Toma, Int. J. Mod. Phys. A **31**, no. 20n21, 1650121 (2016) [arXiv:1505.04665 [hep-ph]]; S. Kanemura, K. Nishiwaki, H. Okada, Y. Orikasa, S. C. Park and R. Watanabe, PTEP **2016**, no. 12, 123B04 (2016) [arXiv:1512.09048 [hep-ph]]; S. Kanemura, O. Seto and T. Shimomura, Phys. Rev. D **84**, 016004 (2011). E. Ma, Phys. Rev. D **73**, 077301 (2006) [hep-ph/0601225]. A. Ahriche, C. S. Chen, K. L. McDonald and S. Nasri, Phys. Rev. D **90**, 015024 (2014) [arXiv:1404.2696 [hep-ph]]. A. Ahriche, K. L. McDonald and S. Nasri, JHEP **1410**, 167 (2014) [arXiv:1404.5917 [hep-ph]]. L. Megreldze and Z. Tavartkiladze, Nucl. Phys. B **914**, 553 (2017) [arXiv:1609.07344 [hep-ph]]. I
- [15] A. Ahriche, K. L. McDonald and S. Nasri, JHEP **1602**, 038 (2016) [arXiv:1508.02607 [hep-ph]]. A. Ahriche, K. L. McDonald and S. Nasri, JHEP **1606**, 182 (2016) [arXiv:1604.05569 [hep-ph]]. I, II B, II B, 2
- [16] M. Aoki, S. Kanemura, K. Sakurai and H. Sugiyama, Phys. Lett. B **763**, 352 (2016) [arXiv:1607.08548 [hep-ph]]. P. Fileviez Perez, T. Han, G. Y. Huang, T. Li and K. Wang, Phys. Rev. D **78**, 071301 (2008) [arXiv:0803.3450 [hep-ph]]. C. S. Chen, C. Q. Geng, J. N. Ng and J. M. S. Wu, JHEP **0708**, 022 (2007) [arXiv:0706.1964 [hep-ph]]. J. Kersten and A. Y. Smirnov, Phys. Rev. D **76**, 073005 (2007) [arXiv:0705.3221 [hep-ph]]. A. Das and N. Okada, Phys. Rev. D **88**, 113001 (2013) [arXiv:1207.3734 [hep-ph]]. D. Atwood, S. Bar-Shalom and A. Soni, Phys. Rev. D **76**, 033004 (2007) [hep-ph/0701005]. S. Antusch, E. Cazzato and O. Fischer, JHEP **1604**, 189 (2016) [arXiv:1512.06035 [hep-ph]]. S. Antusch, E. Cazzato and O. Fischer, Int. J. Mod. Phys. A **32** (2017) no.14, 1750078 [arXiv:1612.02728 [hep-ph]]. I
- [17] A. Ahriche, S. Nasri and R. Soualah, Phys. Rev. D **89**, no. 9, 095010 (2014) [arXiv:1403.5694 [hep-ph]]. C. Guella, D. Cherigui, A. Ahriche, S. Nasri and R. Soualah, Phys. Rev. D **93**, no. 9, 095022 (2016) [arXiv:1601.04342 [hep-ph]]. D. Cherigui, C. Guella, A. Ahriche and S. Nasri, Phys. Lett. B **762**, 225 (2016) [arXiv:1605.03640 [hep-ph]]. S. Y. Ho and J. Tandean, Phys. Rev. D **89**, 114025 (2014) [arXiv:1312.0931 [hep-ph]]. S. Kanemura, T. Nabeshima and H. Sugiyama, Phys. Rev. D **87**, no. 1, 015009 (2013) [arXiv:1207.7061 [hep-ph]]. II
- [18] M. Chekkal, A. Ahriche, A. B. Hammou and S. Nasri, Phys. Rev. D **95**, no. 9, 095025 (2017) [arXiv:1702.04399 [hep-ph]]. I
- [19] M. Lindner, M. Platscher and F. S. Queiroz, arXiv:1610.06587 [hep-ph]. I
- [20] P. Achard *et al.* [L3 Collaboration], Phys. Lett. B **587**, 16 (2004) [hep-ex/0402002]. I, II B, II B
- [21] T. Behnke, C. Damerell, J. Jaros, A. Miyamoto *et al.* (ILC Collaboration), arXiv:0712.2356 [physics.ins-det]. I, III, IV B
- [22] C. Adolphsen *et al.*, arXiv:1306.6328 [physics.acc-ph]. III, IV B

- [23] H. Baer *et al.*, arXiv:1306.6352 [hep-ph]. I, IV B
- [24] M. J. Boland *et al.* [CLIC and CLICdp Collaborations], arXiv:1608.07537 [physics.acc-ph]. I
- [25] T. Suehara and T. Tanabe, Nucl. Instrum. Meth. A **808**, 109 (2016) [arXiv:1506.08371 [physics.ins-det]]. I, III
- [26] C. Drig, K. Fujii, J. List and J. Tian, arXiv:1403.7734 [hep-ex]. I
- [27] Y. Mambrini, Phys. Rev. D **84**, 115017 (2011) [arXiv:1108.0671 [hep-ph]]. X. G. He and J. Tandean, Phys. Rev. D **84**, 075018 (2011) [arXiv:1109.1277 [hep-ph]]. G. Belanger, K. Kannike, A. Pukhov and M. Raidal, JCAP **1301**, 022 (2013) [arXiv:1211.1014 [hep-ph]]. J. M. Cline, K. Kainulainen, P. Scott and C. Weniger, Phys. Rev. D **88**, 055025 (2013) Erratum: [Phys. Rev. D **92**, no. 3, 039906 (2015)] [arXiv:1306.4710 [hep-ph]]. H. Han, J. M. Yang, Y. Zhang and S. Zheng, Phys. Lett. B **756**, 109 (2016) [arXiv:1601.06232 [hep-ph]]. A. Abada, D. Ghaffor and S. Nasri, Phys. Rev. D **83**, 095021 (2011) [arXiv:1101.0365 [hep-ph]]. A. Abada and S. Nasri, Phys. Rev. D **85**, 075009 (2012) [arXiv:1201.1413 [hep-ph]]. I
- [28] A. Ahriche and S. Nasri, Phys. Rev. D **85**, 093007 (2012) [arXiv:1201.4614 [hep-ph]]. I, 1
- [29] A. Birkedal, K. Matchev and M. Perelstein, Phys. Rev. D **70**, 077701 (2004) [hep-ph/0403004]. II
- [30] C. Patrignani *et al.* [Particle Data Group], Chin. Phys. C **40**, no. 10, 100001 (2016). II A, II B, II B, III
- [31] S. Heinemeyer *et al.* [LHC Higgs Cross Section Working Group], arXiv:1307.1347 [hep-ph]. II A
- [32] A. Ahriche and S. Nasri, JCAP **1307**, 035 (2013) [arXiv:1304.2055 [hep-ph]]. II B
- [33] A. Ahriche, K. L. McDonald and S. Nasri, arXiv:1505.04320 [hep-ph]. II B
- [34] T. Toma and A. Vicente, JHEP **1401**, 160 (2014) [arXiv:1312.2840 [hep-ph]]. II B
- [35] J. Hisano, T. Moroi, K. Tobe and M. Yamaguchi, Phys. Rev. D **53**, 2442 (1996) [hep-ph/9510309]. II B
- [36] C. W. Chiang, H. Okada and E. Senaha, Phys. Rev. D **96**, no. 1, 015002 (2017) [arXiv:1703.09153 [hep-ph]]. D. A. Dicus, H. J. He and J. N. Ng, Phys. Rev. Lett. **87**, 111803 (2001) [hep-ph/0103126]. T. Nomura, H. Okada and Y. Orikasa, Phys. Rev. D **94**, no. 5, 055012 (2016) [arXiv:1605.02601 [hep-ph]]. T. Nomura and H. Okada, Phys. Rev. D **94**, 075021 (2016) [arXiv:1607.04952 [hep-ph]]. K. S. Babu and J. Julio, Nucl. Phys. B **841**, 130 (2010) [arXiv:1006.1092 [hep-ph]]. S. Lee, T. Nomura and H. Okada, arXiv:1702.03733 [hep-ph]. II B
- [37] A. M. Baldini *et al.* [MEG Collaboration], Eur. Phys. J. C **76**, no. 8, 434 (2016) [arXiv:1605.05081 [hep-ex]]. II B
- [38] B. Aubert *et al.* [BaBar Collaboration], Phys. Rev. Lett. **104**, 021802 (2010) [arXiv:0908.2381 [hep-ex]]. II B
- [39] K. Hayasaka *et al.*, Phys. Lett. B **687**, 139 (2010) [arXiv:1001.3221 [hep-ex]]. II B, II B
- [40] U. Bellgardt *et al.* [SINDRUM Collaboration], Nucl. Phys. B **299**, 1 (1988). II B
- [41] P. A. R. Ade *et al.* [Planck Collaboration], Astron. Astrophys. **594**, A13 (2016) [arXiv:1502.01589 [astro-ph.CO]]. II B
- [42] A. Semenov, Comput. Phys. Commun. **180**, 431 (2009) [arXiv:0805.0555 [hep-ph]]. II B, II B, 5, IV
- [43] A. Belyaev, N. D. Christensen and A. Pukhov, Comput. Phys. Commun. **184**, 1729 (2013) [arXiv:1207.6082 [hep-ph]]. II B, II B, 5, IV
- [44] E. Accomando *et al.* [CLIC Physics Working Group], hep-ph/0412251. III, IV B
- [45] R.W.Assmann and F. Zimmermann, SNOWMASS-2001-E3014, CERN-SL-2001-064-AP, CERN-CLIC-NOTE-501, CLIC-NOTE-501; W. Liu, W. Gai, L. Rinolfi, and J. Sheppard, Conf.Proc. C100523, THPEC035 (2010). III, IV B
- [46] G. Cowan, K. Cranmer, E. Gross and O. Vitells, Eur. Phys. J. C **71**, 1554 (2011) Erratum: [Eur. Phys. J. C **73**, 2501 (2013)] [arXiv:1007.1727 [physics.data-an]].